Magnetoresistance of Nanoscale Molecular Devices

ODED HOD,[†] ERAN RABANI,*,[†] AND ROI BAER*,[‡]

School of Chemistry, The Sackler Faculty of Exact Science, Tel Aviv University, Tel Aviv 69978, Israel, and Department of Physical Chemistry and the Lise Meitner Center for Quantum Chemistry, the Hebrew University of Jerusalem, Jerusalem 91904, Israel

ABSTRACT

Affecting the current through a molecular or nanoscale junction is usually done by a combination of bias and gate voltages. Magnetic fields are less studied because nanodevices can capture only low values of the magnetic flux. We review recent work done with the aim of finding the conditions for magnetic fields to significantly affect the conductance of such junctions. The basic idea is to create narrow tunneling resonances through a molecular ring-like structure that are highly sensitive to the magnetic field. We describe a computational method that allows us to examine atomistic models of such systems and discuss several specific examples of plausible systems, such as the quantum corral, carbon nanotubes, and polycyclic aromatic hydrocarbon molecules. A unique property of the magnetic field, namely, its ability to split degenerate levels on the ring, is shown to allow prototypes of interesting new nanoscale devices, such as the three-terminal parallel logic gate.

Introduction

Single-molecule electronics[1–12] is a rapidly growing scientific field, although the seeds were planted more than 30 years ago.[13] In recent years, a number of experimental techniques have been developed to synthesize molecular junctions and measure their conductance.[14–25] These systems are often controlled by a gate potential designed to shift conductance peaks into the low-bias regime.[15,26–32] The referred questions are of fundamental nature, leading to the understanding of current–voltage relations.

Due to their small flux, magnetic fields have been rarely used in conjunction with molecular electronics (an exception is the Kondo effect in single-molecule transistors[16,18]). This is in contrast to a related field, electronic transport through mesoscopic devices, where considerable activity

Oded Hod received his B.Sc. from the Hebrew University (1994). He is a graduate student at Tel-Aviv University. His research involves the study of nanomaterials, including mechanical, electronic, and electromagnetic behavior of molecular devices.

Eran Rabani received his Ph.D. from the Hebrew University (1996). After completing postdoctoral work at Columbia University, he joined Tel Aviv University in 1999. He has been an Associate Professor of theoretical chemistry since 2003. His research interests cover nanomaterials, equilibrium and nonequilibrium statistical mechanics, self-assembly, and classical and quantum processes in condensed phases.

Roi Baer received his B.Sc, M.Sc., and Ph.D. (1996) from the Hebrew University of Jerusalem. Following postdoctoral research at the University of California, Berkeley, he joined the Hebrew University in 1998. He has been an Associate Professor of theoretical chemistry since 2001. His research interests include electronic structure, density functional theory, molecular conductance, and quantum molecular dynamics.
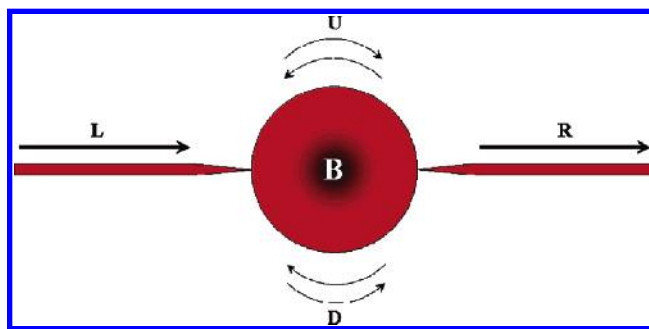
FIGURE 1. An illustration of the Continuum AB interferometer model. A conducting ring is coupled to two conducting wires and placed in a perpendicular magnetic field.

with magnetic fields has led to the discovery of the quantum hall effect[33] and a rich description of transport in such conductors.[34–38] The scarcity of experimental activity is due to the belief that significant magnetic response is obtained only when the magnetic flux is on the order of the *quantum flux*, $\phi_0 = h/q_e$ (where q_e is the electron charge and h is Planck's constant) and attaining such a flux for molecular and nanoscale devices (of typical cross sectional area of square nanometers) requires unrealistically huge magnetic fields. Nevertheless, several interesting experimental studies of the effect of magnetic fields in nanodevices have been published recently.[39–42] Reference 41 showed that an axial magnetic field of a few teslas can affect the conductance along the axis of a 2–5 nm diameter carbon nanotube. This effect was attributed to a 20–40 meV splitting of degenerate rotational angular momentum states around the nanotube axis. Similar findings were reported in ref 40.

Here, we review recent theoretical work[43–45] regarding the essential physical requirements necessary for the construction of nanometer scale magnetoresistance molecular devices. The basic idea is to weakly couple a molecular ring to conducting leads, creating a resonance tunneling junction. The resonant state is tuned by a gate potential to attain maximal conductance in the absence of a magnetic field. The application of a relatively small magnetic field shifts the state out of resonance, and conductance is strongly suppressed. The combination of a gate potential and a magnetic field reveals new features and provides additional conductivity control.

Basic Principles

The primary question to be answered is how to set up a nanoscale device so that the magnetic field can control the current flowing through it. To discuss the basic physical principles involved, let us first regard a simple analytical model. Consider a one-dimensional Aharonov–Bohm[46] (AB) interferometer. It consists of a conducting ring of radius *r* coupled to two conducting wires placed in a perpendicular uniform magnetic field **B** as shown in Figure 1.
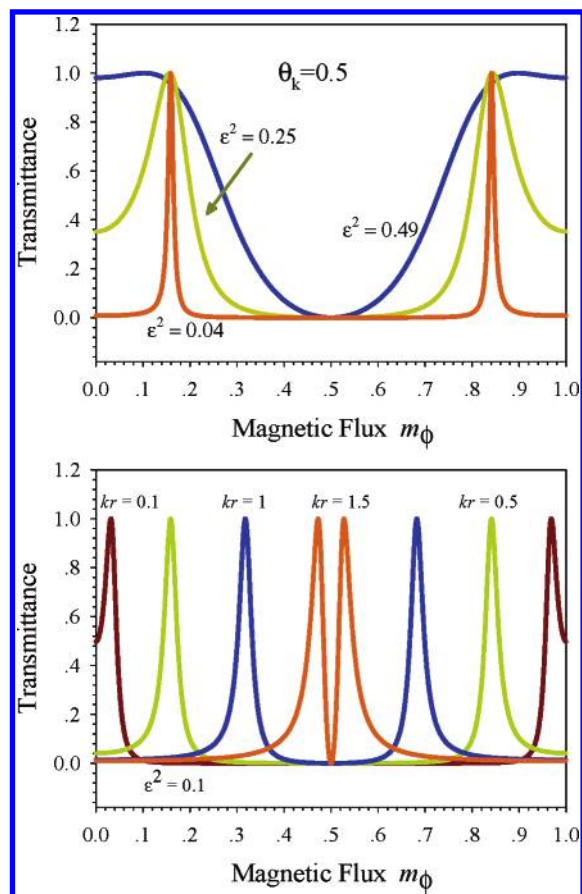
† Tel Aviv University.
‡ Hebrew University of Jerusalem.

FIGURE 2. Transmittance probability as a function of the magnetic flux and its dependence on the coupling strength ϵ^2 (top) and on the spatial phase kr (bottom). Notice that while ϵ^2 controls the width of the peaks, kr controls their position along the AB period.

The relevant Hamiltonian is of an electron in an electromagnetic field:

$$\hat{H} = \frac{(\mathbf{p} - e\mathbf{A})^2}{2\mu} + V(\mathbf{r}) \tag{1}$$

where $\mathbf{A}(\mathbf{r})$ is the vector potential, $\mathbf{B} = \nabla \times \mathbf{A}$, $V(\mathbf{r})$ is the electrostatic potential on the ring, $\mathbf{r}$ is the electron position. We assume $\mathbf{B}$ is a homogeneous field orthogonal to the ring. Consider an electron moving on the left wire as it approaches the left junction. The reflectance probability is $1 - 2\epsilon^2$, where ϵ is the probability amplitude to mount either the upper (U) or lower (D) branch of the ring (henceforth "the coupling"). The ensuing dynamics is described as follows: the part of the wave function that is transmitted into the ring will repeatedly scatter off the right and left junctions. Between each scattering event, the wave function shifts phase. This phase shift is composed of two contributions: the *spatial* phase shift kr, which is the product of the conducting electron wavenumber k and the radius r of the ring, and the *magnetic* phase shift $m_\phi = B\pi r^2/\phi_0$, the dimensionless magnetic flux. The latter contribution is sign sensitive to direction (clockwise or counterclockwise). The wave function bifurcates, so each part of it scatters in a different way and thus gains a different phase. At each scattering event on the left (right) junction, some probability flux will leak to

the left (right) wire. This flux will depend sensitively on the phases, causing an interference pattern on the ring. The total transmittance is the sum of all the flux contributions on the right wire. This transmittance determines the current through the junction.

Using a method due to Gefen, Imry, and Azbel,[47] one can obtain an analytic expression for the transmittance probability through the ring. This expression depends solely on three parameters: the coupling of the ring to the wires ϵ^2, the electron wavenumber k through $\theta_k = kr$, and the dimensionless flux through $\cos(2\pi m_\phi)$. In Figure 2 (upper panel), we present the transmittance vs m_ϕ for several ϵ^2 values at $\theta_k = 0.5$. It is seen that the coupling ϵ^2 controls the *width* of the transmittance peaks: as it is reduced from its maximum $\epsilon^2 = 1/2$, the transmittance peaks narrow (when $\epsilon^2 \rightarrow 0$ each peak becomes a δ-function). Figure 2 (lower panel) shows transmittance when θ_k is changed while ϵ^2 is fixed. Note how θ_k controls the *position* of the transmittance peaks, enabling a shift toward the low-flux regime.

In the weak coupling limit ($\epsilon^2 \approx 0$), the electron scattering wave function on the ring is a linear combination of $\psi_m(\theta) = \exp(im\theta)$, where $m = 0, \pm 1, \pm 2$, etc. corresponding to a wavenumber k_m:

$$rk_m = m \tag{2}$$

Resonance tunneling occurs when the ring energy level, $E_m = \hbar^2(m - m_\phi)^2/(2\mu r^2)$ (μ is the electron effective mass) equals the kinetic energy of the electron on the wire, $\hbar^2 k^2/(2\mu)$:

$$\frac{\hbar^2 k^2}{2\mu} = \frac{\hbar^2(m - m_\phi)^2}{2\mu r^2} \tag{3}$$

To form a resonance at zero magnetic field, one requires that $k = k_m$. Then application of the magnetic field, even if the flux is small, disrupts this resonance condition and reduces the transmittance considerably. For different values of the wavenumber k, the resonance condition in eq 3 will be obtained at different values of the magnetic flux.

While the magnetic fields needed for a full AB period are extremely high, we find that by careful tuning of the conducting wavenumber and coupling between the leads it is possible to have a magnetic field dramatically affecting transmittance and therefore conductance.

Considerations for a Molecular Device

We now discuss the application of the above ideas to more realistic molecular conductors. In molecular junctions, the conductance is mainly affected by electrons near the Fermi level of the leads (assuming both left and right leads are identical and a *very small bias* is applied). Thus in a realistic system, we have no way of controlling k of the incoming electron: it is equal to k_F. On the other hand, the wavenumber of an electron on a ring is quantized, determined solely by ring radius and excitation number (eq 2). Since k_F is constant, we use a gate field on the ring
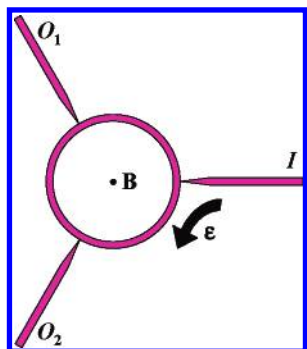
FIGURE 3. A schematic three-terminal device. An electron coming from the input channel I mounts the device with coupling strength ϵ. The magnetic flux controls its specific exit channel, either O_1 or O_2.

to accelerate (or decelerate) the electron as it mounts the ring. The gate potential thus modifies the resonance condition of eq 3 to

$$\frac{\hbar^2 k^2}{2\mu} = \frac{\hbar^2 (m - m_\phi)^2}{2\mu r^2} + V_g \tag{4}$$

Once a gate potential shifts a ring level into resonance with the Fermi energy, the effect of the magnetic field can be understood as follows. At zero magnetic field, the ring level is doubly degenerate (m is positive or negative). The magnetic flux removes this degeneracy and causes each level to split: one level has its energy raised and the other lowered. This shifts the levels out of resonance causing reduction of current. As long as resonance is sharp, even a small magnetic flux ($m_\phi \ll 1$) can affect the transmittance, and positive magnetoresistance is achieved. The resonance width is determined by the lead-ring coupling, which can be controlled by the chemical nature of the molecular junction or by physical manipulation of the separation between the leads and the molecular ring.

Why Use Magnetic Fields?

At this point, the reader may wonder why it is important to use a magnetic field to control the conductance. After all, resonance tunneling is sensitive to other external perturbations, in particular, the gate voltage itself. This is of course true, yet the magnetic field has important properties not shared by gate potentials. For example, it can be used to control the electron's phase, which cannot be altered by a gate potential.

To illustrate this point, consider a three-terminal device, shown in Figure 3, composed of a ring coupled to an input channel I and two output channels O_1 and O_2. Notice the reflection symmetry with respect to the plane passing through wire I, perpendicular to the plane of the ring. Before we describe the exact analytical result for the transmittance probability, let us examine the weak coupling limit. In this limit, the junctions do not affect the wave function on the ring. Thus each output channel can be treated separately. Under proper gating, the magnetic field **B** can shift the conducting state into full resonance, thus increasing the current through O_1. Reversing the
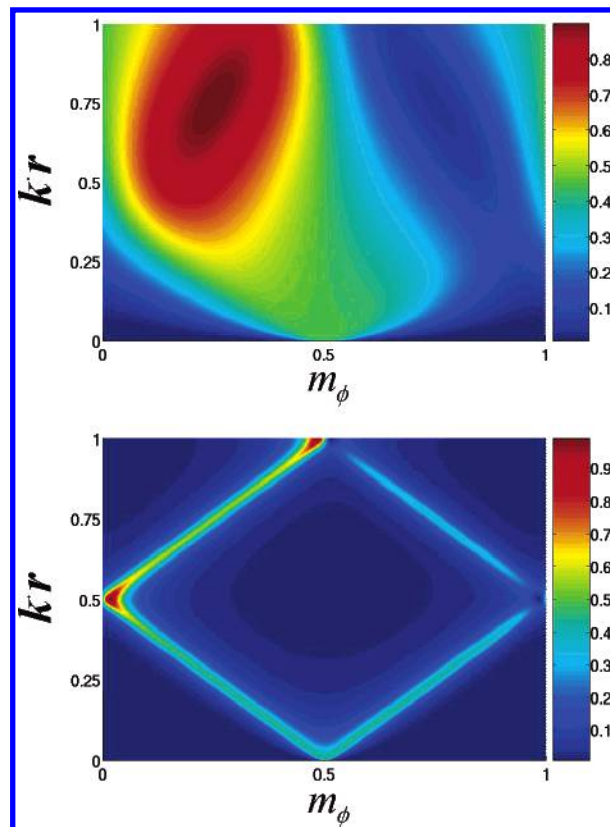

FIGURE 4. The I → O_1 transmittance in the three-terminal device illustrated in Figure 3: upper panel, strong coupling limit ($\epsilon^2 = 0.49$); lower panel, weak coupling limit ($\epsilon^2 = 0.1$). The I → O_2 results are the mirror image of the ones presented here.

polarity of **B** will shift the conducting level away from resonance, thus reducing the current. What happens at the other output channel, O_2? We answer this using a reflection transformation through the symmetry plane. The Hamiltonian of the system is not invariant under such a reflection because of the magnetic field. However, if the reflection is followed by reversal of the direction of the magnetic field, that is, $B \to -B$, then the Hamiltonian is invariant. Under such a composite transformation $O_1 \to O_2$, and we can use our previous analysis for O_1 with one difference: we must reverse the sign of B. Thus, opposite to the O_1 output, the application of a positive magnetic field will *diminish* the conductance through O_2, while a negative magnetic field will *enhance* it.

In Figure 4, we present the transmittance probability[48,49] I → O_1 for strong (upper panel) and weak (lower panel) coupling between the ring and the leads. As in the two-terminal case, when the coupling is strong, the transmittance is broad over a wide range of magnetic fields, and the maxima can be shifted along the magnetic field axis by a change in the conducting electron wavenumber. For low coupling, the transmittance peaks narrow considerably and their position depends on k and m_ϕ linearly. When $kr = 0.5$, the transmittance ($T_1(kr,m_\phi)$) is small but nonnegligible for $m_\phi = 0$, thus we are near resonance. As the magnetic flux is raised above zero (keeping $kr = 0.5$), the transmittance increases rapidly reaching a narrow sharp peak when full resonance is achieved. When m_ϕ is

lowered below zero, the transmittance decreases rapidly to zero. Due to the reflection symmetry discussed above, the result for the I → O_2 terminal is the mirror image of I → O_1, namely, $T_2(kr,-m_\phi) = T_1(kr,m_\phi)$. Thus, as the flux m_ϕ becomes positive, the conductance T_2 will decrease, while as it becomes negative T_2 increases.

In summary, magnetic fields offer unique controllability of nanometer scale interferometer conductance. Their polarity can be used to selectively switch between conducting channels. Such control is more difficult to achieve with scalar potentials lacking the required symmetry-breaking features.

Atomistic Simulation

For realistic molecular conductors, atomistic models are required. The principal tool for this is a magnetic extended Hückel theory (MEHT). Within this approach, we assume a homogeneous magnetic field **B** and add appropriate terms to the extended Hückel Hamiltonian $\hat{H}_{EH}$ based on eq 1 (atomic units are used):

$$\hat{H}_{MEH} = \hat{H}_{EH} + \hat{V}_G - \mu_B \hat{\mathbf{L}} \cdot \hat{\mathbf{B}} + \frac{B^2}{8} r_\perp^2 \qquad (5)$$

Here, $\hat{V}_G$ is the gate potential, raising or lowering the energy of atomic orbitals centered on atoms belonging to the ring (molecular bridge), μ_B is the Bohr magneton, $\hat{\mathbf{L}} = \hat{\mathbf{r}} \times \hat{\mathbf{p}}$ is an angular momentum operator, and $r_\perp$ is the projection of $\mathbf{r} = (x,y,z)$ onto the ring plane perpendicular to **B**. We neglect the spin magnetic moment. Next, Slater type orbitals $|STO\rangle_\alpha$ used in the extended Hückel method are brought to gauge invariant (GI) form,[50] $|GISTO\rangle_\alpha = |STO\rangle_\alpha\, e^{-i(\mathbf{A}_\alpha \cdot \mathbf{r})}$. Here $\mathbf{A}_\alpha = \frac{1}{2}(\mathbf{B}_\alpha \times \mathbf{R}_\alpha)$ is the magnetic vector potential at position $\mathbf{R}_\alpha$, the center of the atomic orbital. As customarily done in the extended Hückel approximation, the basis overlap elements are used to evaluate the matrix elements of the Hamiltonian. Under the London approximation,[51] the overlap and Hamiltonian matrix elements are given by

$$S_{\alpha\beta} = {}_\alpha\langle STO|STO\rangle_\beta\, e^{i\Phi_{\alpha\beta}}$$

and

$$H_{\alpha\beta} = \frac{1}{2}\{{}_\alpha\langle STO|\hat{H}_{MEH}|STO\rangle_\beta\, e^{i\Phi_{\alpha\beta}} + {}_\beta\langle STO|\hat{H}_{MEH}|STO\rangle_\alpha\, e^{i\Phi_{\beta\alpha}}\}$$

where $\Phi_{\alpha\beta} = \frac{1}{2}(\mathbf{A}_\alpha - \mathbf{A}_\beta)(\mathbf{R}_\alpha + \mathbf{R}_\beta)$ is the gauge factor evaluated at the midpoint between the two atoms. Once the Hamiltonian matrix is set up, the electronic energy levels are extracted by solving the generalized eigenvalue problem $\hat{H}c = E\hat{S}c$. The conductance is calculated using the Landauer formalism,[52] in which the junction conductance g is determined by the Fermi level transmittance $T(\epsilon_F)$, $g = g_0 T(\epsilon_F)$, where $g_0 = 2q_e^2/h$. The transmittance is evaluated using the trace formula: $T(E) = \text{tr}[G\Gamma_L G^a \Gamma_R]$. This formula is employed using two approaches: the first approach is the non-equilibrium Green's function (NEGF) formalism,[53] where G^r (G^a) is the retarded (advanced)
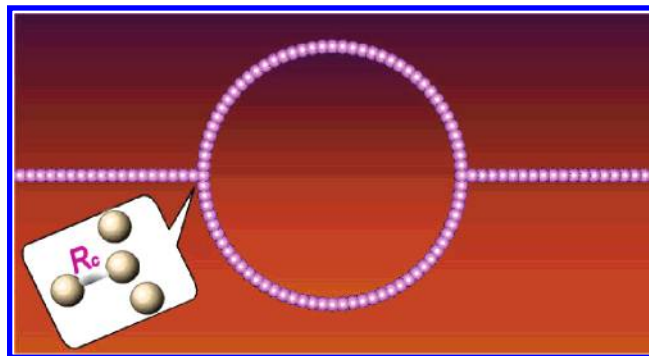

FIGURE 5. An illustration of an atomic corral junction composed of 40 copper atoms. The inset describes the coupling of the atomic wire to the corral. Reproduced with permission from ref 43. Copyright 2004 American Chemical Society.

Green's function and Γ_L (Γ_R) is the imaginary part of the self-energy of the left (right) lead, computed using an iterative procedure.[54] The second approach is similar, but the Γ are negative imaginary potentials[55] added to the left (right) leads. The parameters for these are chosen so that electrons with kinetic energies in a wide band around $k_F^2/2$ (where k_F is the Fermi momentum in the metal) are effectively absorbed.[56]

Utilizing these computational tools, we next report results for a selection of nanoscale molecular systems for which pronounced magnetoresistance phenomena are predicted at feasible magnetic fields.

Magnetic Switching in a Quantum Corral

A detailed study of the magnetoresistance of an atomic corral, illustrated in Figure 5, is given in ref 43. Here we review the main results. We consider a corral of copper atoms on a metal oxide surface. Atoms are placed with bond distance of 2.35 Å; experimental realization of this setup can be achieved using scanning tunneling microscopy (STM) techniques.[57−59]

All copper atoms are treated explicitly; each contributes one s-electron and 10 d-electrons. The valence 4s, 4p, and 3d atomic orbitals are explicitly considered in the Hamiltonian. The Cu s conduction band is half-filled, so the Fermi wavelength equals four bond lengths. Thus symmetric loops can be classified into two groups, those containing $4N$ and $4N + 2$ atoms.

In Figure 6, we plot the conductance through the Cu corral as a function of the magnetic field **B** and the gate potential V_g for the two prototype corrals with $N = 10$. The full AB period for the two prototypes is, respectively, 600 and 540 T. For a given magnetic flux intensity, there are two conductance peaks, corresponding to the split of two degenerate electronic levels as discussed above. Change of the gate potential shifts the conductance maxima, similar to the effect of changing the wavenumber in the continuum model. By adjustment of the gate potential, it is possible to tune the resonance such that the transmittance is maximal at zero magnetic flux.

To illustrate switching, we need to control the width of the conductance resonances. In the continuum model,
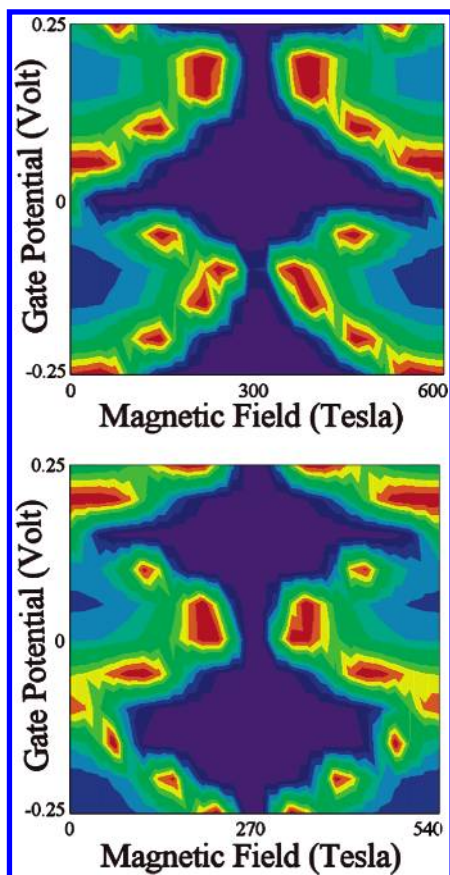
FIGURE 6. Conductance as a function of magnetic field and gate voltage at $T = 1$ K for a ring of 40 (top) and 42 (bottom) Cu atoms ($\sim$3 nm diameter). The image uses a rainbow color code: red corresponds to $g = g_0$ and purple to $g = 0$. Reproduced with permission from ref 43. Copyright 2004 American Chemical Society.

FIGURE 7. The conductance of 40 (upper panel) and 42 (lower panel) Cu atom corrals at $T = 1$ K as a function of the magnetic field and the contact bond length R_c. The gate potential is 0 V (upper panel) and -0.13 V (lower panel). Reproduced with permission from ref 43. Copyright 2004 American Chemical Society.

this was done by reducing the coupling ϵ^2. In the molecular system, this is achieved by increasing the distance between the atomic corral and the molecular wires, R_c. Alternatively, one can introduce an impurity atom at the junctions between the wires and the ring by doping the contacts.[42] For quantum corrals, the former approach seems more realistic.

In Figure 7, the conductance as a function of the magnetic field is depicted for several values of R_c for the two generic system sizes. For each system, a proper gate potential is chosen to ensure maximal conductance at zero magnetic field. As R_c is increased, the sensitivity of the conductance to the magnetic field increases. At the highest leads−ring separation studied, we achieve switching capability of with $\sim$1 T, a feasible magnetic field.

Nanotube Magnetic Switch

A simpler geometry of a nanometric magnetic switch is based on a single-walled carbon nanotube (SWCNT). The magnetic field is oriented along the axis of the tube, and we discuss the *circumferential* conductance. Two experimental configurations are considered. The first consists of a nanotube placed on an insulating substrate between two thin conducting contacts (see Figure 8a), and a bias potential is applied between the contacts. Similar setups
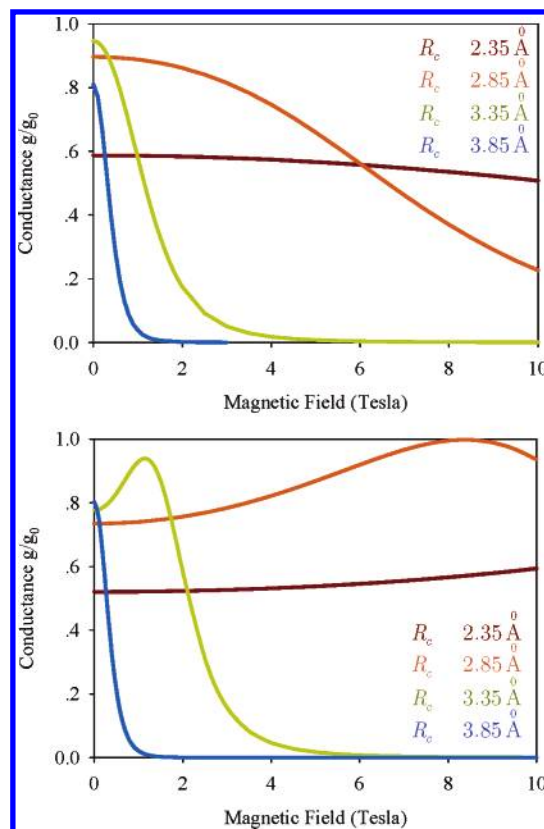
have been recently demonstrated experimentally.[18,60,61] In the second configuration, a nanotube is placed on a conducting substrate coupled to a STM tip from above as described schematically in Figure 8b. The bias potential is applied between the STM tip and the underlying surface.[62,63] Related calculations on similar setups were published recently.[64,65] Using the magnetic extended Hückel approach described above, we calculate the resulting conductance between the leads for both configurations. In the calculation, all carbon atoms of the tube are treated explicitly; each carbon atom contributes two 2s-electrons and two 2p-electrons. For configuration a, both leads are modeled by atomic conducting wires, while for configuration b, the STM tip is modeled by a semi-infinite one-dimensional atomic conducting gold wire and the substrate by a semi-infinite slab of atomic gold crystal. The calculations were conducted for a tube containing four unit cells, using minimum image periodic boundary conditions for the passivation of the edge atoms. Tests on longer tubes reveal the same qualitative picture.

In the upper panel of Figure 9, the conductance g through a (24,0) nanotube, calculated for configuration a, is plotted against the magnetic field **B** for several values of the bias potential V_b. For $V_b = 0$, the conductance increases as **B** is increased (negative magnetoresistance), peaks near **B** = 10 T, and subsequently decreases, vanishing at **B** $\geq$ 30 T. The maximum conductance is $g/g_0 = 2$.
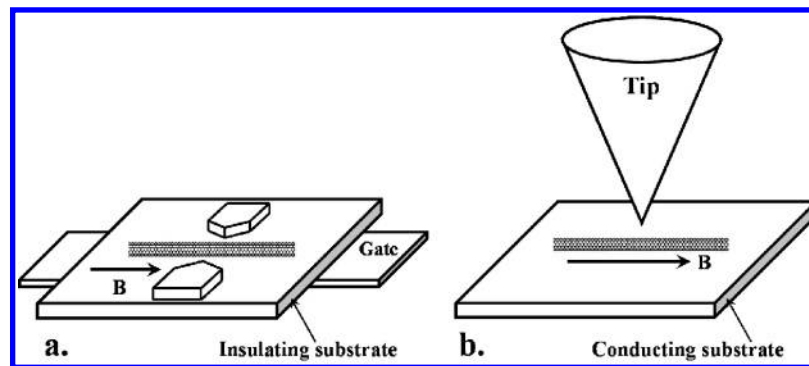
FIGURE 8. The experimental configurations for cross-sectional magnetoresistance of a nanotube: (a) the SWCNT is placed on an insulating surface between two narrow metallic contacts; (b) the SWCNT is placed on a conducting substrate and approached from above by an STM tip. Reproduced with permission from from ref 45. Copyright 2005 American Institute of Physics.

As in the corral example, to achieve switching capability at magnetic fields smaller than 1 T, it is necessary to move the conductance peak to zero magnetic field and at the same time reduce its width. When a small bias is applied to the sample, the conductance peak splits into a doublet. This split corresponds to our assumption that the bias potential drops sharply and equally at both ends of the molecule.[66] The position of the corresponding peaks depends on the value of V_b, and as seen in the figure, it is possible to shift one of the conductance peaks toward low values of **B** such that g is maximal at when **B** = 0. The shift in the conductance peak can be attributed to the change in the energy level through which conductance occurs. As a result of this change, the electron momentum changes as in the case of the atomic corral.

In the lower panel of Figure 9, the effect of changing the tube-contact separation at constant bias potential is studied. As the separation increases, the tube−contact
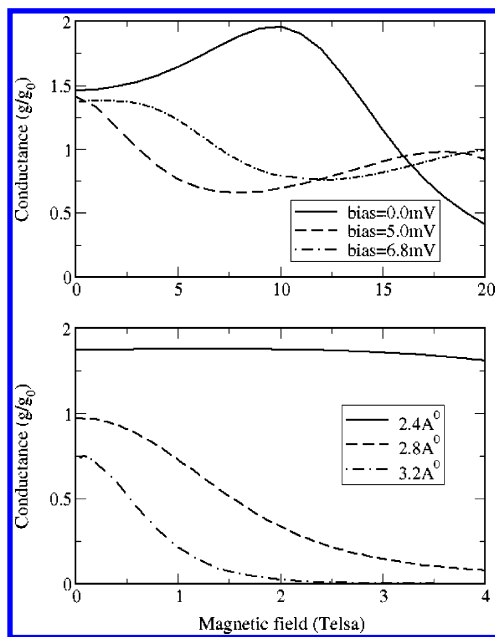
coupling decreases reducing the width of the resonance. Thus, conductance becomes sensitive to the applied magnetic field, and small variations in the field shift the relevant energy level out of resonance, as discussed above. In the magnetoresistance spectrum, this is translated to a narrowing of the transmittance peaks. At the highest separation studied (3.2 Å), the width of the conductance peak is comparable to 1 T.

A similar picture arises when one considers configuration b of Figure 8. In Figure 10, we plot the conductance for a (6,0) SWCNT placed between a sharp STM tip and a conducting surface for two bias voltages. The separation between the nanotube and the conducting leads used in this calculation is 4.1 Å. As can be seen, when a bias voltage of $V_b \approx 0.224$ V is applied the conductance peaks at **B** $\approx$ 14 T. When the bias is changed to $V_b \approx 0.225$ V, the conductance peak shifts toward **B** = 0. Under these conditions, switching occurs at a magnetic field of ~5 T. The higher value of the magnetic field needed to switch this device is a result of the small diameter of the present tube.

The study of axial conductance in carbon nanotubes and the effects of magnetic fields on the conductance has recently received considerable attention.[40−42] In addition to these studies, we propose to utilize the *circumferential*

FIGURE 9. Conductance versus the magnetic field for a (24,0) nanotube as computed for configuration a in Figure 8: upper panel, the effect of bias potential on position of conductance peaks at constant tube−contacts separation of 2.4 Å; lower panel, the effect of decreasing the tube−contact coupling at constant bias potential V_g = 6.8 mV. Adapted from ref 45.
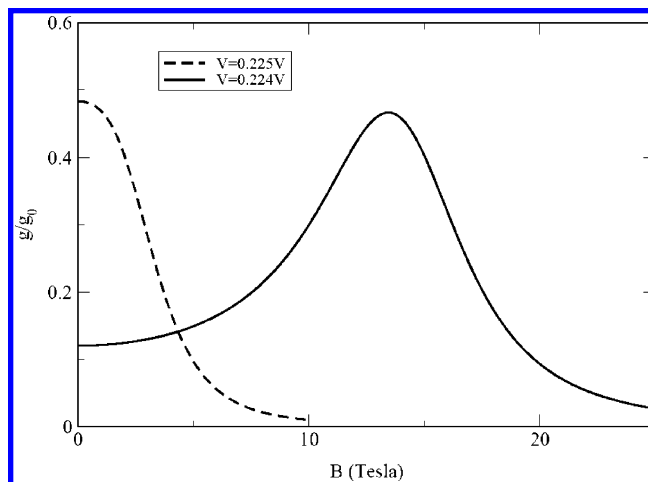

FIGURE 10. Conductance vs magnetic field through a (6,0) nanotube as calculated for configuration b in Figure 8. Reproduced with permission from from ref 45. Copyright 2005 American Institute of Physics.
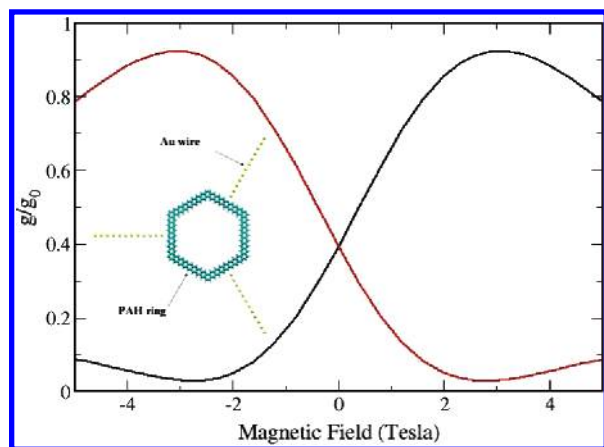
FIGURE 11. Conductance as a function of the magnetic field for the three-terminal molecular switch. The inset shows the PAH molecular ring coupled to three gold wires.

conductance, which we believe is more sensitive to magnetic fields, since the relevant density of conducting states is smaller. Carbon nanotubes can be used as electromagnetic elements but also as magnetic sensors. Furthermore, since the effects depend on the chirality of the nanotubes, magnetic fields can be used to characterize the structure of the nanotubes.[42]

Multiprocessing Logic Gate

An interesting case in which magnetic fields provide a unique control over conductance is based on the three-terminal setup described above. Here, we study the effects of magnetic field polarity on the selective switching of molecular devices useful for parallel logic operations.[44]

Using the detailed atomistic MEHT approach, we study a polycyclic aromatic hydrocarbon (PAH) hexagonal ring composed of 48 conjugated benzene units, forming a hexagonal ring of diameter ∼3 nm, coupled to three gold atomic wires (see the inset in Figure 11). In Figure 11, we plot the conductance of the molecular switch as a function of the magnetic field intensity for both output channels (black and red curves). A relatively large gate voltage, V_g ≈ 1.85 V, is needed to bring the system into resonance, and the lead–molecule separation is taken to be ∼3 Å. For **B** = 0, both channels are semi-opened and the conductance is $0.4g_0$ at the selected gate voltage. When a field of ∼2.5 T is applied, one output channel opens while the other closes. As the polarity of the field changes sign these two channels interchange roles. This is similar to the continuum model discussed above.

On the basis of these results, it is possible to design a molecular logic gate that processes two different logic operations in parallel. This can be achieved by choosing one input signal as the bias voltage (V_b) and the other input signal as the magnetic field (**B**). For the bias input signal, V_b, we mark as 0 the case where $V_b = 0$ and as 1 the case where a small bias is applied. For the magnetic field input signal, we mark as 0 the case where $B \approx -2.5$ T and as 1 the case where $B \approx 2.5$ T. The output signals are the currents measured through the two output chan-

nels O_1 and O_2. The following truth table (Table 1) can be built on the basis of these definitions:

Table 1. Truth Table for the Parallel Molecular Logic Gate

V_b	**B**	O_1	O_2
0	0	0	0
0	1	0	0
1	0	0	1
1	1	1	0

One sees that the output O_1 gives the logic operation I AND B while O_2 corresponds to I AND $\bar{B}$ (the over-bar stands for NOT). The truth table holds for a wide range of magnetic field intensities $\pm(2-4)$ T and is thus suitable for robust logic gate operations. Shifting the conductance peaks via the change of the bias potential will give rise to different logic operations of the same setup.

Summary and Perspectives

We have studied magnetic field effects on conductance in nanometer molecular rings. We showed that by decreasing the coupling to the leads and adjusting a gate voltage one can increase the sensitivity to magnetic fields on the order of a few tesla. This result is remarkable since a full AB period involves fluxes large by 2 orders of magnitude. The magnetoresistance sensitivity increases as the diameter of the circular device grows. The advantage of using magnetic fields was demonstrated through the possibility to selectively switch different conducting channels of a system, enabling the construction of logic gate devices on the molecular scale.

Small devices are relatively insensitive to temperature effects[43] because of the large spacing of electronic states. This is different from mesoscopic systems where experiments are performed on the subkelvin regime because of the large density of electronic states and the relatively small dephasing length scales at higher temperatures. The temperature dependence in the smaller devices will be due to electron–phonon coupling, which is stronger in small systems, especially under resonant tunneling conditions. The extent to which this will affect our results is now being studied in our groups.

It is conceivable that these ideas can also be used to construct sensitive magnetic field nanoscale sensors. In a sensor, one does not need full switching, so these devices are sensitive to even smaller magnetic fields.

References

(1) Jortner, J.; Ratner, M. *Molecular Electronics*; Blackwell Science Inc: New York, 1997.
(2) Nitzan, A. Electron transmission through molecules and molecular interfaces. *Annu. Rev. Phys. Chem.* **2001**, *52*, 681−750.
(3) Emberly, E. G.; Kirczenow, G. Theory of electrical conduction through a molecule. *Mol. Electron.: Sci. Technol.* **1998**, *852*, 54−67.
(4) Ratner, M. Molecular electronics − Pushing electrons around. *Nature* **2000**, *404*, 137−138.

(5) Pantelides, S. T.; Di Ventra, M.; Lang, N. D. Molecular electronics by the numbers. *Physica B* **2001**, *296*, 72–77.

(6) Roth, C.; Joachim, C. *Atomic and Molecular Wires*; Kluwer: Dordrecht, The Netherlands, 1997.

(7) Joachim, C.; Gimzewski, J. K.; Aviram, A. Electronics using hybrid-molecular and mono-molecular devices. *Nature* **2000**, *408*, 541–548.

(8) Nitzan, A.; Ratner, M. A. Electron transport in molecular wire junctions. *Science* **2003**, *300*, 1384–1389.

(9) Avouris, P. Molecular electronics with carbon nanotubes. *Acc. Chem. Res.* **2002**, *35*, 1026–1034.

(10) Dekker, C. Carbon nanotubes as molecular quantum wires. *Phys. Today* **1999**, *52*, 22–28.

(11) Heath, J. R.; Ratner, M. A. Molecular electronics. *Phys. Today* **2003**, *56*, 43–49.

(12) Tour, J. M. Molecular electronics. Synthesis and testing of components. *Acc. Chem. Res.* **2000**, *33*, 791–804.

(13) Aviram, A.; Ratner, M. A. Molecular Rectifiers. *Chem. Phys. Lett.* **1974**, *29*, 277.

(14) Tans, S. J.; Devoret, M. H.; Dai, H. J.; Thess, A.; Smalley, R. E.; Geerligs, L. J.; Dekker, C. Individual single-wall carbon nanotubes as quantum wires. *Nature* **1997**, *386*, 474–477.

(15) Reed, M. A.; Zhou, C.; Muller, C. J.; Burgin, T. P.; Tour, J. M. Conductance of a molecular junction. *Science* **1997**, *278*, 252–254.

(16) Park, J.; Pasupathy, A. N.; Goldsmith, J. I.; Chang, C.; Yaish, Y.; Petta, J. R.; Rinkoski, M.; Sethna, J. P.; Abruna, H. D.; McEuen, P. L.; Ralph, D. C. Coulomb blockade and the Kondo effect in single-atom transistors. *Nature* **2002**, *417*, 722–725.

(17) Hersam, M. C.; Guisinger, J. W. Silicon-based molecular nanotechnology. *Nanotechnology* **2000**, *11*, 70–76.

(18) Liang, W. J.; Shores, M. P.; Bockrath, M.; Long, J. R.; Park, H. Kondo resonance in a single-molecule transistor. *Nature* **2002**, *417*, 725–729.

(19) Weber, H. B.; Reichert, J.; Weigend, F.; Ochs, R.; Beckmann, D.; Mayor, M.; Ahlrichs, R.; von Lohneysen, H. Electronic transport through single conjugated molecules. *Chem. Phys.* **2002**, *281*, 113–125.

(20) Kergueris, C.; Bourgoin, J. P.; Palacin, S.; Esteve, D.; Urbina, C.; Magoga, M.; Joachim, C. Electron transport through a metal-molecule-metal junction. *Phys. Rev. B* **1999**, *59*, 12505–12513.

(21) Cui, X. D.; Primak, A.; Zarate, X.; Tomfohr, J.; Sankey, O. F.; Moore, A. L.; Moore, T. A.; Gust, D.; Harris, G.; Lindsay, S. M. Reproducible measurement of single-molecule conductivity. *Science* **2001**, *294*, 571–574.

(22) Kushmerick, J. G.; Holt, D. B.; Yang, J. C.; Naciri, J.; Moore, M. H.; Shashidhar, R. Metal-molecule contacts and charge transport across monomolecular layers: Measurement and theory. *Phys. Rev. Lett.* **2002**, *89*, No. 086802.

(23) Slowinski, K.; Fong, H. K. Y.; Majda, M. Mercury–mercury tunneling junctions. 1. Electron tunneling across symmetric and asymmetric alkanethiolate bilayers. *J. Am. Chem. Soc.* **1999**, *121*, 7257–7261.

(24) Selzer, Y.; Cai, L. T.; Cabassi, M. A.; Yao, Y. X.; Tour, J. M.; Mayer, T. S.; Allara, D. L. Effect of local environment on molecular conduction: Isolated molecule versus self-assembled monolayer. *Nano Lett.* **2005**, *5*, 61–65.

(25) Smit, R. H. M.; Noat, Y.; Untiedt, C.; Lang, N. D.; van Hemert, M. C.; van Ruitenbeek, J. M. Measurement of the conductance of a hydrogen molecule. *Nature* **2002**, *419*, 906–909.

(26) Zhitenev, N. B.; Meng, H.; Bao, Z. Conductance of small molecular junctions. *Phys. Rev. Lett.* **2002**, *88*, No. 226801.

(27) Klein, D. L.; Roth, R.; Lim, A. K. L.; Alivisatos, A. P.; McEuen, P. L. A single-electron transistor made from a cadmium selenide nanocrystal *Nature* **1997**, *389*, 699–701.

(28) Tans, S. J.; Verschueren, A. R. M.; Dekker, C. Room-temperature transistor based on a single carbon nanotube. *Nature* **1998**, *393*, 49–52.

(29) Yao, Z.; Postma, H. W. C.; Balents, L.; Dekker, C. Carbon nanotube intramolecular junctions. *Nature* **1999**, *402*, 273–276.

(30) Chen, J.; Reed, M. A.; Rawlett, A. M.; Tour, J. M. Large on–off ratios and negative differential resistance in a molecular electronic device. *Science* **1999**, *286*, 1550–1552.

(31) Postma, H. W. C.; Teepen, T.; Yao, Z.; Grifoni, M.; Dekker, C. Carbon nanotube single-electron transistors at room temperature. *Science* **2001**, *293*, 76–79.

(32) Cui, Y.; Lieber, C. M. Functional nanoscale electronic devices assembled using silicon nanowire building blocks. *Science* **2001**, *291*, 851–853.

(33) von Klitzing, K.; Dorda, G.; Pepper, M. New method for high-accuracy determination of the fine-structure constant based on quantized Hall resistance. *Phys. Rev. Lett.* **1980**, *45*, 494–497.

(34) Webb, R. A.; Washburn, S.; Umbach, C. P.; Laibowitz, R. B. Observation of H/E Aharonov-Bohm Oscillations in Normal-Metal Rings *Phys. Rev. Lett.* **1985**, *54*, 2696–2699.

(35) Timp, G.; Chang, A. M.; Cunningham, J. E.; Chang, T. Y.; Mankiewich, P.; Behringer, R.; Howard, R. E. Observation of the Aharonov-Bohm Effect for Omega-C–Tau Greater Than 1. *Phys. Rev. Lett.* **1987**, *58*, 2814–2817.

(36) van Oudenaarden, A.; Devoret, M. H.; Nazarov, Y. V.; Mooij, J. E. Magneto-electric Aharonov-Bohm effect in metal rings. *Nature* **1998**, *391*, 768–770.

(37) Yacoby, A.; Heiblum, M.; Mahalu, D.; Shtrikman, H. Coherence and Phase-Sensitive Measurements in a Quantum-Dot. *Phys. Rev. Lett.* **1995**, *74*, 4047–4050.

(38) Auslaender, O. M.; Yacoby, A.; de Picciotto, R.; Baldwin, K. W.; Pfeiffer, L. N.; West, K. W. Tunneling spectroscopy of them elementary excitations in a one-dimensional wire. *Science* **2002**, *295*, 825–828.

(39) Bachtold, A.; Strunk, C.; Salvetat, J. P.; Bonard, J. M.; Forro, L.; Nussbaumer, T.; Schonenberger, C. Aharonov-Bohm oscillations in carbon nanotubes. *Nature* **1999**, *397*, 673–675.

(40) Zaric, S.; Ostojic, G. N.; Kono, J.; Shaver, J.; Moore, V. C.; Strano, M. S.; Hauge, R. H.; Smalley, R. E.; Wei, X. Optical signatures of the Aharonov-Bohm phase in single-walled carbon nanotubes. *Science* **2004**, *304*, 1129–1131.

(41) Minot, E.; Yaish, Y.; Sazonova, V.; McEuen, P. L. Determination of electron orbital magnetic moments in carbon nanotubes. *Nature* **2004**, *428*, 536.

(42) Cao, J.; Wang, Q.; Rolandi, M.; Dai, H. J. Aharonov-Bohm interference and beating in single-walled carbon-nanotube interferometers. *Phys. Rev. Lett.* **2004**, *93*.

(43) Hod, O.; Rabani, E.; Baer, R. Feasible Nanometric Magnetoresistance Devices. *J. Phys. Chem. B* **2004**, *108*, 14807–14810.

(44) Hod, O.; Rabani, E.; Baer, R. A Parallel Electromagnetic Molecular Logic Gate. *J. Am. Chem. Soc.* **2005**, *127*, 1648–1649.

(45) Hod, O.; Rabani, E.; Baer, R. Magnetoresistance Devices Based on Single Walled Carbon Nanotubes. *J. Chem. Phys.* **2005**, *123*, No. 051103.

(46) Aharonov, Y.; Bohm, D. Significance of electromagnetic potentials in the quantum theory. *Phys. Rev.* **1959**, *115*, 485–491.

(47) Gefen, Y.; Imry, Y.; Azbel, M. Y. Quantum Oscillations and the Aharonov-Bohm Effect for Parallel Resistors *Phys. Rev. Lett.* **1984**, *52*, 129–132.

(48) Wu, C. H.; Ramamurthy, D. Logic functions from three-terminal quantum resistor networks for electron wave computing. *Phys. Rev. B* **2002**, *65*.

(49) Ryu, C. M.; Cho, S. Y.; Shin, M.; Park, K. W.; Lee, S. J.; Lee, E. H. Quantum waveguide theory for triply connected Aharonov-Bohm rings. *Int. J. Mod. Phys. B* **1996**, *10*, 701–712.

(50) Pople, J. A. Molecular Orbital Theory of Diamagnetism: I. An Approximate LCAO Scheme. *J. Chem. Phys.* **1962**, *37*, 53–xx.

(51) London, F. Quantum theory of interatomic currents in aromatic compounds. *J. Phys. Radium* **1937**, *8*, 397–409.

(52) Imry, Y.; Landauer, R. Conductance viewed as transmission. *Rev. Mod. Phys.* **1999**, *71*, S306–S312.

(53) Xue, Y. Q.; Datta, S.; Ratner, M. A. First-principles based matrix Green's function approach to molecular electronic devices: general formalism. *Chem. Phys.* **2002**, *281*, 151–170.

(54) Lopez-Sancho, M. P.; Lopez-Sanchos, J. M.; Rubio, J. Highly convergent schemes for the calculation of bulk and surface green functions. *J. Phys. F* **1985**, *15*, 851.

(55) Neuhasuer, D.; Baer, M. The Time-Dependent Schrodinger-Equation – Application of Absorbing Boundary-Conditions. *J. Chem. Phys.* **1989**, *90*, 4351–4355.

(56) Baer, R.; Neuhauser, D. Phase coherent electronics: A molecular switch based on quantum interference. *J. Am. Chem. Soc.* **2002**, *124*, 4200–4201.

(57) Bartels, L.; Meyer, G.; Rieder, K. H. Lateral manipulation of single Cu atoms on flat and stepped copper surfaces. *J. Vac. Sci. Technol. A* **1998**, *16*, 1047–1049.

(58) Manoharan, H. C.; Lutz, C. P.; Eigler, D. M. Quantum mirages formed by coherent projection of electronic structure. *Nature* **2000**, *403*, 512–515.

(59) Nazin, G. V.; Qiu, X. H.; Ho, W. Visualization and Spectroscopy of a Metal-Molecule-Metal Bridge. *Science* **2003**, *302*, 77–81.

(60) Deshmukh, M. M.; Prieto, A. L.; Q, G.; H, P. Fabrication of Asymmetric Electrode Pairs with Nanometer Separation Made of Two Distinct Metals. *Nano Lett.* **2003**, *3*, 1383–1385.

(61) Biercuk, M. J.; Mason, N.; Martin, J.; Yacoby, A.; Marcus, C. M. Anomalous conductance quantization in carbon nanotubes. *Phys. Rev. Lett.* **2005**, *94*.

(62) Zhang, Z.; Lieber, C. M. Nanotube Structure and Electronic-Properties Probed by Scanning-Tunneling-Microscopy. *Appl. Phys. Lett.* **1993**, *62*, 2792–2794.

(63) Collins, P. G.; Zettl, A.; Bando, H.; Thess, A.; Smalley, R. E. Nanotube nanodevice. *Science* **1997**, *278*, 100−103.

(64) Zhang, G.; Cao, Z. L.; Gu, B. L. Tunneling transport in STM-tip-nanotube-substrate systems. *Mod. Phys. Lett. B* **2000**, *14*, 717−724.

(65) Zhang, G.; Cao, Z. L.; Gu, B. L. The influence of temperature and magnetic field on the tunneling transport in STM-tip-nano-tube-substrate systems. *Mod. Phys. Lett. B* **2000**, *14*, 1065−1072.

(66) Nitzan, A.; Galperin, M.; Ingold, G. L.; Grabert, H. On the electrostatic potential profile in biased molecular wires. *J. Chem. Phys.* **2002**, *117*, 10837−10841.